Revision 3

Anisotropic growth of olivine during crystallization in basalts from Hawaii: Implications for olivine fabric development

DA-PENG WEN[1], YONG-FENG WANG[1,2]*, JUN-FENG ZHANG[1,2], AND ZHEN-MIN JIN[1]

[1]State Key Laboratory of Geological Processes and Mineral Resources, School of Earth Sciences, China University of Geosciences, Wuhan 430074, China

[2]Global Tectonic Center, School of Earth Sciences, China University of Geosciences, Wuhan 430074, China

*Corresponding author:

Tel.: +86-18971577987

Fax: +86-27-67883002

Email addresses:

wendapeng@cug.edu.cn (Da-Peng Wen)

yfwang@cug.edu.cn (Yong-Feng Wang)

jfzhang@cug.edu.cn (Jun-Feng Zhang)

zmjin@cug.edu.cn (Zhen-Min Jin)

ABSTRACT

Olivine fabrics are crucial for deciphering anisotropy of many physical properties in the upper mantle, such as seismic velocity and thermal diffusivity. Under circumstances where crystallized mantle rocks don't suffer strong modification from later deformation, olivine fabrics can reflect the results of anisotropic crystal growth and viscous magmatic flow. Currently little is known about the crystallization habits of olivine in nature. Here we report crystallization habits of olivine phenocrysts in two Hawaii tholeiitic basalts. The low Mg numbers (< 88.1) of olivine grains suggest that they are crystallized products from the host magma rather than captured ones from peridotite xenoliths. Many olivine grains have non-equidimensional euhedral crystal shapes due to anisotropic crystal growth rates. Electron backscatter diffraction (EBSD) analyses show that of the 115 analyzed olivine grains, 84 grains are oriented with their long axes parallel to the [001]-axis, while 24 and 7 grains have their long axes parallel to the [100]-axis and the [010]-axis, respectively. This growth habit is different from that reported for olivine grown at subsolidus conditions without fluid/melt. Our results imply that olivine will most likely form the AG-type fabric during crystallization from magma chambers undergoing compaction, and the B-type fabric during pure or simple shear mode magmatic flow, provided that no or weak later plastic deformation superimposes on these magmatic fabrics. The AG-type and the B-type olivine fabrics in natural cumulates can be interpreted as results of anisotropic growth of olivine and viscous magmatic flow. Anisotropic olivine growth is expected to strongly affect the fabric development in the upper mantle portion where there is extensive partial melting (e.g., the mantle wedge above subduction zones or the upper mantle beneath the middle ocean ridges) or reactive melt percolation leading to crystallization of olivine at the consumption of pyroxene.

Keywords: olivine fabric, crystallographic preferred orientation, anisotropic growth, cumulate

INTRODUCTION

Crystallographic preferred orientation (CPO) of minerals is important for extrapolating deformation mechanism, shear sense, strain geometry, deformation temperature of rocks from deep crust and upper mantle of the Earth (e.g., Law 1990). It is generally believed that significant CPOs of minerals are produced by dislocation glide during dislocation creep of rocks (e.g., Zhang and Karato 1995; Tommasi et al. 2000; Zhang et al. 2006; Soustelle et al. 2010; Michibayashi and Oohara 2013). In addition, remarkable CPOs may also result from grain-size sensitive creep regimes, like diffusion creep or grain boundary sliding (GBS) (e.g., Bons and den Brok 2000; Hansen et al. 2012; Miyazaki et al. 2013; Getsinger and Hirth 2014; Précigout and Hirth 2014), although many studies have linked weak or random CPOs of minerals to deformation by diffusion creep or grain boundary sliding as well (e.g., Storey and Prior 2005; Warren and Hirth 2006; Skemer and Karato 2008; Drury et al. 2011). Apart from deformation-induced CPOs, distinct mineral CPOs are also frequently seen in undeformed rocks, like granites, anorthosites, gabbros, and peridotites of magmatic origin (e.g., Jackson et al. 1975; Benn and Allard 1989; Mainprice and Nicolas 1989; Müller et al. 2011; Ji et al. 2014; VanTongeren et al. 2015). These magmatic CPOs are crucial for understanding the dynamical processes within magma chambers (e.g., Benn and Allard 1989) and to better constrain the CPO development and deformation mechanisms of deformed magmatic rocks, considering that CPOs arising from magmatic flow could be preserved during later deformation by grain-size sensitive flow (e.g., Cao et al. 2017), but destroyed during strong deformation by dislocation creep. Thus, knowledge of CPO formation under supersolidus conditions is of significance.

Olivine is the most abundant and probably the weakest constituent mineral in the upper mantle (Mackwell et al. 1990). Numerous efforts have been made to elaborate olivine CPOs during deformation in nature and laboratory experiments (e.g., Avé Lallemant 1975; Zhang and Karato 1995; Bystricky et al. 2000; Jung and Karato 2001; Tommasi et al. 2008; Ohuchi et al. 2011). These studies demonstrated that olivine CPOs in response to dislocation creep vary as a function of temperature, stress, water content, pressure, and melt, in addition to deformation geometry. For instance, olivine develops fabrics characterized by the [001] axes parallel to the shear direction and the [010] axes or the [100] axes normal to the shear plane under water-rich conditions (i.e., the B- and C-type, respectively), and forms fabrics featured by the [100] axes parallel to the lineation and the [010] axes normal to the foliation under water-poor conditions (i.e., the A-type) (Jung and Karato 2001).

In comparison, considerably fewer studies had been dedicated to clarify how olivine CPO will develop under supersolidus (magmatic) conditions (Benn and Allard 1989; Zetterström 1996; Jousselin et al. 2012). Although olivine also show distinct CPOs under supersolidus conditions, such as the AG-type (also known as the [010]-fiber pattern; i.e., the [010] axes form a point maximum normal to the foliation plane, and the [100] and the [001] axes both form a great girdle in the foliation plane; see Mainprice 2007; Tommasi et al. 2008) or the B-type, they cannot be linked to plastic deformation and explained by existing hypotheses, but are related to the crystal shape of olivine crystallized from magmas. Therefore, the crystallization habits of olivine during magma cooling can cast lights on olivine fabric development in olivine-bearing magmatic rocks. Many studies have explored in detail the textural evolution and compositions of olivine crystallized from magmas through experiments and natural observations (e.g., Donaldson 1976; Faure et al. 2003a, b; Faure et al. 2007; Welsch et al. 2013; Welsch et al. 2014). However, these studies mainly focused on the morphology and textures of olivine phenocrysts. Statistical analyses of growth habits of olivine are absent.

In this study, we carried out a detailed study on olivine phenocrysts from two Hawaii basalts. The mineral chemistry evidence is presented to demonstrate that the phenocrystic olivine was derived from fractional crystallization of the host basalts. Then the evidence of oriented growth of olivine phenocrysts preferentially along their [001]-axis over the [100]- and the [010]-axis is reported. Finally, the significance of anisotropic growth of olivine crystals for fabric development in cumulates is discussed.

SAMPLES AND METHODS

Two vesicular Hawaii basalts, one from the O'ahu Island and the other from the Big

Island, were collected for this study. They are both tholeiitic lavas with MgO of 46.99-47.38 wt% and $Na_2O + K_2O$ of 1.49-2.61 wt% (see the supplementary Table S1). Nine thin sections with a final polishing of 0.05 μm by colloidal Al_2O_3 had been prepared from these two samples. The major-element compositions of olivine phenocrysts were determined using a JEOL Superprobe JXA-8100 electron microprobe at the Institute of Geology and Geophysics, Chinese Academy of Sciences. The analyses were conducted at an accelerating voltage of 15 kV, a beam current of 20 nA, and a spot diameter of 5 μm. The counting time for SiO_2, MgO, FeO was 20 s on peak and 10 s on lower and upper background positions. The counting time for other elements was 40 s on peak and 20 s on lower and upper background positions. All elements were detected by five analyzing crystals: two TAP crystals for Si, Mg, Al and Na, two LIFH crystals for Fe, Ni, Mn and Cr, and one PETJ crystal for K, Ca and Ti, respectively. SPI standard olivine-34 and diopside-21 were used as monitor standards. The detection limits for all elements are 100-200 ppm. The precision (1SD) is 0.4-1.0% for major elements (Si, Mg and Fe), 3-9% for minor elements (Ca, Mn and Ni), and 19-90% for trace elements (Al, Ti, Cr, K and Na).

To clarify the anisotropic growth behavior of olivine during crystallization from magmas, we selected those euhedral and anisometric olivine grains. Some rounded olivine grains can sometimes be observed in these samples. However, they are neglected because it is difficult to determine their long/short axes and aspect ratios although they may also represent crystallization products from magma (Welsch et al. 2013). The crystal orientations of selected olivine grains were determined by indexation of electron backscatter diffraction (EBSD) patterns using a Quanta 450 field emission gun scanning electron microscope (FEG-SEM) at the State Key Laboratory of Geological Processes and Mineral Resources, China University of Geosciences (Wuhan). The 'match unit' for olivine in our HKL software is a forsterite with a Pbnm space group (lattice parameters of the unit cell are a = 4.76 Å, b = 10.21 Å, and c = 5.98 Å). The measurements were conducted with an accelerating voltage of 20 kV, a working distance of 24-25 mm, and a spot size of 6. Diffraction patterns were collected manually and indexed using the HKL Channel 5 + software. Only those measurements with mean angular deviation (MAD) values below 1.0 (between detected and simulated Kikuchi bands) were accepted and recorded. Moreover, the corresponding backscatter electron (BSE) image for each measured grain was also saved at the same time.

The crystal orientations of olivine phenocrysts are presented by stereographic projection of the [100], [010], and [001] axes measured by EBSD. To derive the true growth aspect ratios between two perpendicular crystallographic axes, only those stereographic projections with the third crystallographic axis projected approximately in the center (<10° to the center) are chosen for comparison with the corresponding BSE images. In such cases, the aspect ratio can be easily determined.

RESULTS AND DISCUSSION

Under a petrographic microscope, the studied olivine grains (0.2-3.6 mm in length) are all euhedral, tabular, and free of signs indicative of intracrystalline plastic deformation, like undulose extinction and subgrains (Fig. 1). Sometimes, inclusions of basaltic glass or plagioclase can be observed within olivine (Figs. 1c and 1d). These features clearly demonstrate that these olivine grains grew from the host basalts.

18 olivine phenocrysts from the studied Hawaii basalts have been analyzed for the major-element compositions (see the Supplementary Table S2). They show a considerable compositional variation with MgO contents ranging from 41.97 wt% to 47.60 wt% and FeO contents varying between 11.43 wt% and 18.67 wt% (Fig. 2). The Mg number (= Mg/[Mg + Fe_{total}] × 100 atomic ratios) values of olivine range from 80.0 to 88.1, with most of them falling below 86.0 (Supplementary Table S2). They are generally richer in FeO and more depleted in MgO compared with those from peridotite xenoliths entrained by the Hawaii basalts (e.g., Clague 1988; Sen 1988; Fig. 2), indicating that the olivine phenocrysts are crystallization products from the Hawaii basalts during cooling, rather than relics of captured peridotite xenoliths.

The crystallographic orientations of 546 randomly selected euhedral olivine phenocrysts were determined. Among them 115 olivine grains with one crystallographic axis projected approximately close to the center (i.e., normal to the thin section surface) are chosen to derive the growth aspect ratios between two crystallographic axes. These 115 grains can be divided into three groups: 1) 42 grains with the [100]-axis normal to the thin section surface (Group #1), 2) 46 grains with the [010]-axis normal to the thin section surface (Group #2), and 3) 27 grains with the [001]-axis normal to the thin section surface (Group #3) (Fig. 3 and Table 1). For Group #1 olivine grains, the long axes are always the [001]-axis and the short axes are always the [010]-axis with an average aspect ratio of 1.7 ± 0.6 (error represents two times the standard deviation; Fig. 4a). For group #2 olivine grains, the majority (42 out of 46 grains) shows also the [001] axes being the long axes while the [100] axes being the short axes (with a corresponding average aspect ratio of 1.6 ± 0.7; Fig. 4b). The long axes of rest 4 grains (8.7%; aspect ratios of 1.2-1.7) are the [100]-axis. For Group #3 olivine grains, the long axes of 20 out of 27 grains are the [100] axes (average aspect ratio = 1.4 ± 0.4; Fig. 4c) while those of the rest (aspect ratios ranging from 1.3 to 2.3) are the [010] axes. The observed crystal faces for these olivine grains include {021}, and rarely, {101}, {120} and {110}, in addition to the low-index crystal faces {010}, {100}, and {001} (Fig. 3). These crystal faces were also observed for tabular olivines from peridotite xenoliths, which were explained as growth in the presence of grain boundary fluid (see Drury and van Roermund, 1989).

In summary, the EBSD analyses show that olivine, like many other minerals from the crust and the upper mantle, also grows anisotropically during crystallization in magma chambers. Our measurements demonstrate unambiguously that olivine phenocrysts grown from the Hawaii basalts have mostly a short prism shape with growth of the [001]-axis preferred relative to the [100]- and the [010]-axis and that of the [100]-axis preferred relative to the [010]-axis (Table 1). The preferential growth of the [001]-axis over the other two axes has also been reported by several previous studies (Donaldson 1976; Miyazaki et al. 2013; Welsch et al. 2013).

Previous studies have shown that olivines with euhedral, tabular morphology are common in natural mantle peridotites (e.g., Boullier and Nicolas 1973, 1975; Drury and van Roermund 1989; Vauchez et al. 2005; Vonlanthen et al. 2006; Tommasi et al. 2008). Generally, these olivines are considered to form as a result of grain growth under subsolidus conditions, assisted by the presence of fluid/melt (e.g., Boullier and Nicolas 1975; Drury and van Roermund 1989; Vauchez et al. 2005). Existing observations suggest that, although differing in growth environments (for instance, free space, available constituents, etc.), olivine growth under subsolidus conditions is also anisotropic (e.g., Drury and van Roermund 1989; Tommasi et al. 2008; Miyazaki et al. 2013). Nevertheless, the growth habits of olivine are still poorly constrained. For example, Drury and van Roermund (1989) found that the olivine crystal faces formed at subsolidus conditions are similar to those formed from a fluid phase, but they didn't investigate the specific growth habits of olivine. Tommasi et al. (2008) suggested that the Tok tabular harzburgites experienced selective grain growth during static recrystallization in the presence of melt, forming tabular olivine crystals flattening normal to the

[010]-axis and a strong [010]-fiber CPO. These observations suggest clearly that the [010]-axis is the shortest axis during static recrystallization of olivine in the Tok harzburgites, but it is still not clear from their results the aspect ratios between the [100]- and the [010]-axes. One way to determine the growth habits of euhedral, tabular olivine in natural peridotites is via the CPOs of these olivines by assuming that the CPOs are results of anisotropic growth of olivine. Under such an assumption, the A-type olivine CPOs reported in Drury and van Roermund (1989) and Vauchez et al. (2005) for tabular olivines imply that olivine grows preferentially with $a > c > b$, while the [010]-fiber CPOs reported by Tommasi et al. (2008) imply that olivine grows preferentially with $a > c > b$ or $c > a > b$. Therefore, no exclusive conclusions on the growth habits of olivine under subsolidus conditions can be reached based on the current dataset. Moreover, the driving forces (reduction of interface free energy, reduction of stored energy associated with defects, or chemically induced grain boundary migration; see Evans et al. 2001) for grain growth/recrystallization of olivine are generally not clearly stated by previous studies (e.g., Vauchez et al. 2005; Vonlanthen et al. 2006; Tommasi et al. 2008), which makes the discussion on the controlling factors for anisotropic growth of olivine very difficult. In summary, the general picture for the growth habits of olivine in the presence of fluid/melt is currently far from complete due to data limitation except that the [010]-axis seems to be generally the shortest axis (e.g., Tommasi et al. 2008). On the other hand, for olivine growth in the absence of fluid/melt, Miyazaki et al. (2013) concluded based on experimental observations that olivine grows anisotropically with $a >$

b > *c* at T < 1250 ºC and with *a* > *c* > *b* at T > 1250 ºC, pointing out a different growth habit of olivine under subsolidus conditions from what we observed in Hawaii basalts under supersolidus conditions.

IMPLICATIONS

Olivine crystallization under supersolidus conditions is common in the Earth's upper mantle where there is extensive partial melting, such as the mantle wedge above a subducting slab and the upper mantle beneath a middle ocean ridge, or a reactive melt percolation zone with the crystallization of subhedral to euhedral olivine at the expense of pyroxene (e.g., Vauchez et al., 2005; Tommasi et al., 2008). Anisotropic olivine growth is expected to play an important role in fabric development under these circumstances. Therefore, the crystallization habit of olivine has an immediate influence on olivine fabric development in a magma chamber or channel. In a static magma chamber, gravitational sinking (similar to a compaction deformation) will cause the largest crystal face, i.e., the (010)-plane, of most crystallized olivine grains to align horizontally to form the magmatic foliation, whereas the [100] and the [001] axes will spread in the foliation plane, thus shaping an AG-type or a [010]-fiber olivine fabric (Fig. 5a). In a magma channel undergoing continuous pure shear viscous flow, it is reasonable to expect that the longest axis, i.e., the [001]-axis, will orient preferentially parallel to the flow direction, whereas the [010]-axis will be aligned normal to the flow plane (Fig. 5b). Crystallized olivine grains in a magma channel undergoing simple shear viscous flow will form a similar olivine CPO with the [001] axes and the (010) planes oblique in an acute angle to the shear direction and the shear plane, respectively (Fig. 5c). This fabric pattern is analogous to the B-type olivine fabric that had been demonstrated experimentally to be formed by the (010)[001] slip during dislocation creep of olivine under hydrous or high-pressure conditions (e.g., Jung and Karato 2001; Jung et al. 2009; Ohuchi et al. 2011). The B-type olivine fabric is crucial to the interpretation of upper mantle structure and dynamics, yet many mechanisms have been proposed to interpret its origin under different geological settings, including slip system transition induced by high water contents or high pressure (e.g., Jung and Karato, 2001; Ohuchi et al., 2011), strain partitioning between melt-rich and melt-deficient zones (Holtzman et al., 2003), diffusion creep controlled by interface reaction (Sundberg and Cooper, 2008), grain boundary sliding (Précigout and Hirth, 2014), static topotactic growth of olivine after high-temperature breakdown of foliated serpentinite (Nagaya et al., 2014), and low-temperature dissolution creep (Liu et al., 2018). Our results provide another alternative explanation for the formation of B-type olivine fabric in nature, i.e., oriented alignment of anisometric olivine grains resulting from anisotropic growth. A similar hypothesis has been recently proposed for the asymmetric B-type olivine CPO in the Songshugou dunite cumulates (Cao et al., 2017). Getsinger and Hirth (2014) showed that oriented grain growth and rigid grain rotation during diffusion creep led to significant SPO (shape preferred orientation) and CPO in amphibole growing from a basalt. Because anisotropic grain growth usually leads to a significant SPO, which helps to stabilize grain rotation and prevent destruction of former CPOs (Wheeler, 2009, 2010), the resultant CPOs could be preserved during later diffusion-mediated creep (diffusion creep or diffusion-accommodated GBS) deformation. This mechanism can explain CPOs of olivine in natural peridotites deformed by the diffusion-mediated creep (e.g., Précigout and Hirth, 2014; Cao et al., 2017).

ACKNOWLEDGEMENTS

D. Wen thanks Liang Yuan for help during preparation of thin sections. We are also grateful to Yi Chen for help with the electron microprobe analyses and to Shan-Rong Zhao for helpful discussion. Two anonymous reviewers and the editors, Julia Hammer and Keith Putirka, are greatly thanked for constructive and insightful reviews. This work was supported by the National Natural Science Foundation of China (grant numbers 41372224, 41590623).

REFERENCES CITED

Avé Lallemant, H.G. (1975) Mechanisms of preferred orientations of olivine in tectonite peridotite. Geology, 3, 653–656.

Benn, K., and Allard, B. (1989) Preferred mineral orientations related to magmatic flow in ophiolite layered gabbros. Journal of Petrology, 30, 925–946.

Bons, P.D., and den Brok, B. (2000) Crystallographic preferred orientation development by dissolution-precipitation creep. Journal of Structural Geology, 22, 1713–1722.

Boullier, A.M., and Nicolas, A. (1973) Texture of peridotite nodules from kimberlite at Mothae, Thaba Putsoa and kimberley. In P.H. Nixon, Ed., Lesotho Kimberlites, 55–66.

Boullier, A.M., and Nicolas, A. (1975) Classification of textures and fabrics of peridotite xenoliths from South African Kimberlites. Physics and Chemistry of the Earth, 9, 467–476.

Bystricky, M., Kunze, K., Burlini, L., and Burg, J.-P. (2000) High shear strain of olivine aggregates: Rheological and seismic consequences. Science, 290, 1564–1567.

Cao, Y., Jung, H., and Song, S. (2017) Olivine fabrics and tectonic evolution of fore-arc mantles: A natural perspective from the Songshugou dunite and harzburgite in the Qinling orogenic belt, central China. Geochemistry, Geophysics, Geosystems, 18, doi: 10.1002/2016GC006614.

Clague, D.A. (1988) Petrology of ultramafic xenoliths from Loihi Seamount, Hawaii. Journal of Petrology, 29, 1161–1186.

Donaldson, C.H. (1976) An experimental investigation of olivine morphology. Contributions to Mineralogy and Petrology, 57, 187–213.

Drury, M.R., and van Roermund, H.L.M. (1989) Fluid assisted recrystallization in upper mantle peridotite xenoliths from Kimberlites. Journal of Petrology, 30, 133–152.

Drury, M.R., Avé Lallemant, H.G., Pennock, G.M., and Palasse, L.N. (2011) Crystal preferred orientation in peridotite ultramylonites deformed by grain size sensitive creep, Étang de Lhers, Pyrenees, France. Journal of Structural Geology, 33, 1776–1789.

Evans, B., Renner, J., and Hirth, G. (2001) A few remarks on the kinetics of static grain growth in rocks. International Journal of Earth Sciences, 90, 88–103.

Faure, F., Trolliard, G., Nicollet, C., and Montel, J.-M. (2003a) A developmental model of olivine morphology as a function of the cooling rate and the degree of undercooling. Contributions to Mineralogy and Petrology, 145, 251–263.

Faure, F., Trolliard, G., and Soulestin, B. (2003b) TEM investigation of forsterite dendrites. American Mineralogist, 88, 1241–1250.

Faure, F., Schiano, P., Trolliard, G., Nicollet, C., and Soulestin, B. (2007) Textural evolution of polyhedral olivine experiencing rapid cooling rates. Contributions to Mineralogy and Petrology, 153, 405–416.

Getsinger, A.J., and Hirth, G. (2014) Amphibole fabric formation during diffusion creep and the rheology of shear zones. Geology, 42, 535–538.

Hansen, L.N., Zimmerman, M.E., and Kohlstedt, D.L. (2011) Grain boundary sliding in San Carlos olivine: Flow law parameters and crystallographic-preferred orientation. Journal of Geophysical Research, 116, B08201, doi:10.1029/2011JB008220.

Hansen, L.N., Zimmerman, M.E., and Kohlstedt, D.L. (2012) The influence of microstructure on deformation of olivine in the grain-boundary sliding regime. Journal of Geophysical Research, 117, B09201, doi: 1029/2012JB009305.

Holtzman, B.K., Kohlstedt, D.L., Zimmerman, M.E., Heidelbach, F., Hiraga, T., and Hustoft, J. (2003) Melt segregation and strain partitioning: Implications for seismic anisotropy and mantle flow. Science, 301, 1227–1230.

Jackson, E.D., Green, H.W. II, and Moores, E.M. (1975) The Vourinos ophiolite, Greece: Cyclic units of lineated cumulates overlying harzburgite tectonite. Geological Society of American Bulletin, 86, 390–398.

Ji, S., Shao, T., Salisbury, M.H., Sun, S., Michibayashi, K., Zhao, W., Long, C., Liang, F., and Satsukawa, T. (2014) Plagioclase preferred orientation and induced seismic anisotropy in mafic igneous rocks. Journal of Geophysical Research, 119, doi: 10.1002/2014JB011352.

Jousselin, D., Morales, L.F.G., Nicolle, M., and Stephant, A. (2012) Gabbro layering induced by simple shear in the Oman ophiolite Moho transition zone. Earth and Planetary Science Letters, 331–332, 55–66.

Jung, H., and Karato, S.-I. (2001) Water-induced fabric transitions in olivine. Science, 293, 1460–1463.

Jung, H., Mo, W., and Green, H.W. II (2009) Upper mantle seismic anisotropy resulting from pressure-induced slip transition in olivine. Nature Geoscience, 2, 73–77.

Law, R.D. (1990) Crystallographic fabrics: A selective review of their applications to research in structural geology. In R.J. Knipe, and E.H. Rutter, Eds., Deformation Mechanisms, Rheology and Tectonics, 54, p. 335–352. Geological Society Special Publication, London.

Liu, W., Zhang, J., and Barou, F. (2018) B-type olivine fabric induced by low temperature dissolution creep during serpentinization and deformation in mantle wedge.

Tectonophysics, 722, 1–10.

Mackwell, S.J., Bai, Q., and Kohlstedt, D.L. (1990) Rheology of olivine and the strength of the lithosphere. Geophysical Research Letters, 17, 9–12.

Mainprice, D. (2007) Seismic anisotropy of the deep earth from a mineral and rock physics perspective. Treatise on Geophysics, 2, 437–491.

Mainprice, D., and Nicolas, A. (1989) Development of shape and lattice preferred orientations: Application to the seismic anisotropy of the lower crust. Journal of Structural Geology, 11, 175–189.

Michibayashi, K., and Oohara, T. (2013) Olivine fabric evolution in a hydrated ductile shear zone at the Moho Transition Zone, Oman Ophiolite. Earth and Planetary Science Letters, 377–378, 299–310.

Miyazaki, T., Sueyoshi, K., and Hiraga, T. (2013) Olivine crystals align during diffusion creep of Earth's upper mantle. Nature, 502, 321–326.

Müller, A., Leiss, B., Ullemeyer, K., and Breiter, K. (2011) Lattice-preferred orientations of late-Variscan granitoids derived from neutron diffraction data: Implications for magma emplacement mechanism. International Journal of Earth Sciences, 100, 1515–1532.

Nagaya, T., Wallis, S.R., Kobayashi, H., Michibayashi, K., Mizukami, T., Seto, Y., Miyake, A., and Matsumoto, M. (2014) Dehydration breakdown of antigorite and the formation of B-type olivine CPO. Earth and Planetary Science Letters, 387, 67–76.

Ohuchi, T., Kawazoe, T., Nishihara, Y., Nishiyama, N., and Irifune, T. (2011) High pressure and temperature fabric transitions in olivine and variations in upper mantle seismic anisotropy. Earth and Planetary Science Letters, 304, 55–63.

Précigout, J., and Hirth, G. (2014) B-type olivine fabric induced by grain boundary sliding. Earth and Planetary Science Letters, 395, 231–240.

Sen, G. (1988) Petrogenesis of spinel lherzolite and pyroxenite suite xenoliths from the Koolau shield, Oahu, Hawaii: Implications for petrology of the post-eruptive lithosphere beneath Oahu. Contributions to Mineralogy and Petrology, 100, 61–91.

Skemer, P., and Karato, S.-I. (2008) Sheared lherzolite xenoliths revisited. Journal of Geophysical Research, 113, B07205, doi:10.1029/2007JB005286.

Soustelle, V., Tommasi, A., Demouchy, S., and Ionov, D.A. (2010) Deformation and fluid-rock interaction in the supra-subduction mantle: Microstructures and water contents in peridotite xenoliths from the Avacha volcano, Kamchatka. Journal of Petrology, 51, 363–394.

Storey, C.D., and Prior, D.J. (2005) Plastic deformation and recrystallization of garnet: A mechanism to facilitate diffusion creep. Journal of Petrology, 46, 2593–2613.

Sundberg, M., and Cooper, R.F. (2008) Crystallographic preferred orientation produced by diffusional creep of harzburgite: Effects of chemical interactions among phases during plastic flow. Journal of Geophysical Research, 113, B12208. doi:10.1029/2008JB005618.

Tommasi, A., Mainprice, D., Canova, G., and Chastel., Y. (2000) Viscoplastic self-consistent and equilibrium-based modeling of olivine lattice preferred orientations: Implications for the upper mantle seismic anisotropy. Journal of Geophysical Research, 105, 7893–7908.

Tommasi, A., Vauchez, A., and Ionov, D.A. (2008) Deformation, static recrystallization, and reactive melt transport in shallow subcontinental mantle xenoliths (Tok Cenozoic volcanic field, SE Siberia). Earth and Planetary Science Letters, 272, 65–77.

VanTongeren, J.A., Hirth, G., and Kelemen, P.B. (2015) Constraints on the accretion of the gabbroic lower oceanic crust from plagioclase lattice preferred orientation in the Samail ophiolite. Earth and Planetary Science Letters, 427, 249–261.

Vauchez, A., Dineur, F., and Rudnick, R. (2005) Microstructure, texture and seismic anisotropy of the lithospheric mantle above a mantle plume: Insights from the Labait volcano xenoliths (Tanzania). Earth and Planetary Science Letters, 232, 295–314.

Warren, J.M., and Hirth, G. (2006) Grain size sensitive deformation mechanisms in naturally deformed peridotites. Earth and Planetary Science Letters, 248, 438–450.

Welsch, B., Faure, F., Famin, V., Baronnet, A., and Bachèlery, P. (2013) Dendritic crystallization: A single process for all the textures of olivine in basalts? Journal of Petrology, 54, 539–574.

Welsch, B., Hammer, J., and Hellebrand, E. (2014) Phosphorus zoning reveals dendritic architecture of olivine. Geology, 42, 867–870.

Wheeler, J. (2009) The preservation of seismic anisotropy in the Earth's mantle during diffusion creep. Geophysical Journal International, 178, 1723–1732.

Wheeler, J. (2010) Anisotropic rheology during grain boundary diffusion creep and its relation to grain rotation, grain boundary sliding and superplasticity. Philosophical Magazine, 90, 2841–2864.

Zetterström, L. (1996) Fabric studies of layered igneous rocks from Rum, Scotland, 69p. M. Sc. thesis, Stockholm University.

Zhang, S., and Karato, S.-I. (1995) Lattice preferred orientation of olivine aggregates deformed in simple shear. Nature, 375, 774–777.

Zhang, J., Green, H.W. II, and Bozhilov, K.N. (2006) Rheology of omphacite at high temperature and pressure and significance of its lattice preferred orientations. Earth and Planetary Science Letters, 246, 432–443.

Figure Captions

Fig. 1. Photomicrographs showing the typical euhedral and anisometric olivine (Ol) phenocrysts within the Hawaii basalts. Note the inclusions of plagioclase (Pl) (c) and basaltic glass (d) inside the olivine phenocrysts. Scale bars 1 mm.

Fig. 2. Co-variation diagram of MgO versus FeO for olivine (Ol). Data source: Ol pheonocrysts in the Hawaii basalts (this study); Ol grains in peridotite xenoliths entrained by the Hawaii basalts (Claque 1988; Sen 1988).

Fig. 3. Photomicrographs showing the euhedral olivine phenocrysts and their corresponding crystal orientations determined by EBSD. The crystal faces for these olivines are also indicated. The olivines in a) and b) belong to the Group #1, while those in c) and d) belong to the Group #2 and Group #3, respectively.

Fig. 4. Histograms showing the long/short axis ratios for each group of olivine phenocrysts.

Fig. 5. Schematic olivine fabrics. a. The AG-type olivine fabric that can form by compaction or gravitational sinking of euhedral olivine in a magma chamber. b. The B-type olivine fabric that can form during pure shear magmatic flow. c. The B-type olivine CPO that can form in response to viscous magmatic flow in simple shear. The

foliation plane (S) is normal to the paper along the dashed line, while the lineation (L) is horizontal and trends along the dashed line.

Table 1

Summary of EBSD analyses.

Planes parallel to the thin section surface	(100) (Group #1)		(010) (Group #2)		(001) (Group #3)	
Long axis	[010]	[001]	[100]	[001]	[100]	[010]
Grains	0	42	4	42	20	7

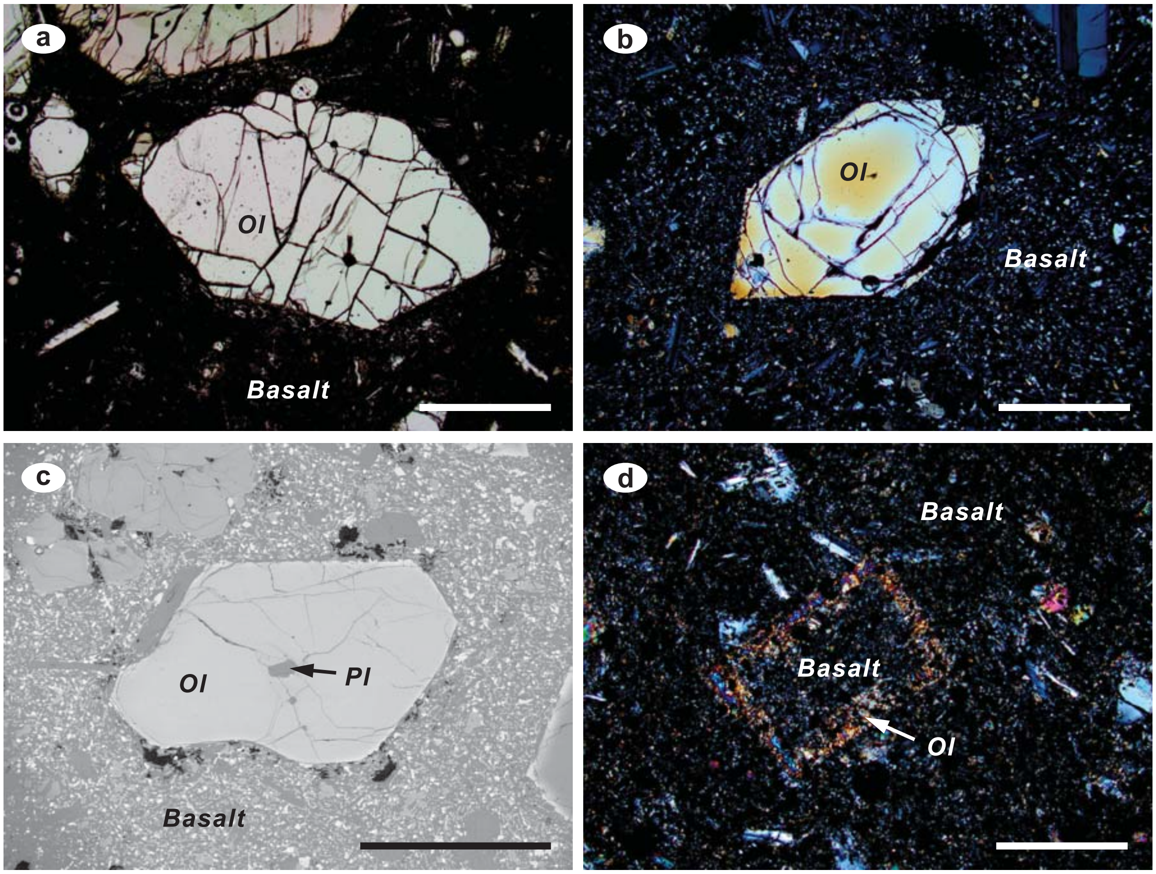

Fig. 1

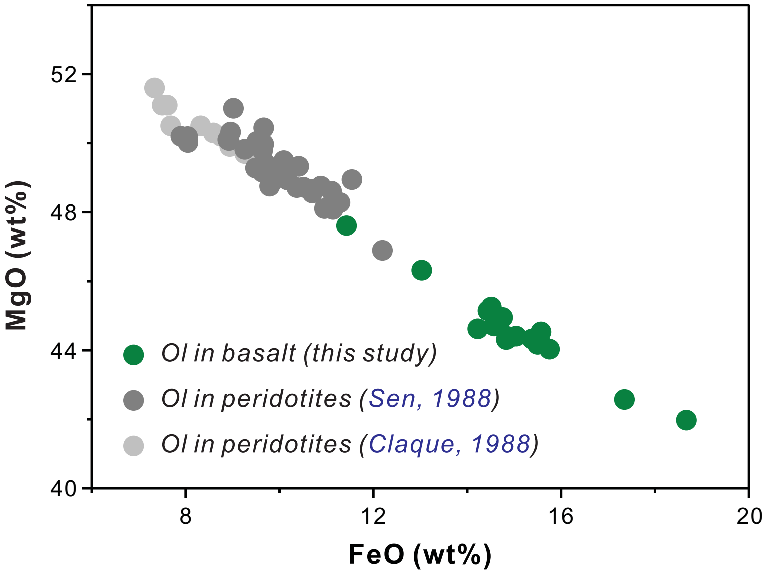
52
48
44
40
MgO (wt%)
8
12
16
20
FeO (wt%)
Ol in basalt (this study)
Ol in peridotites (Sen, 1988)
Ol in peridotites (Claque, 1988)

Fig. 2

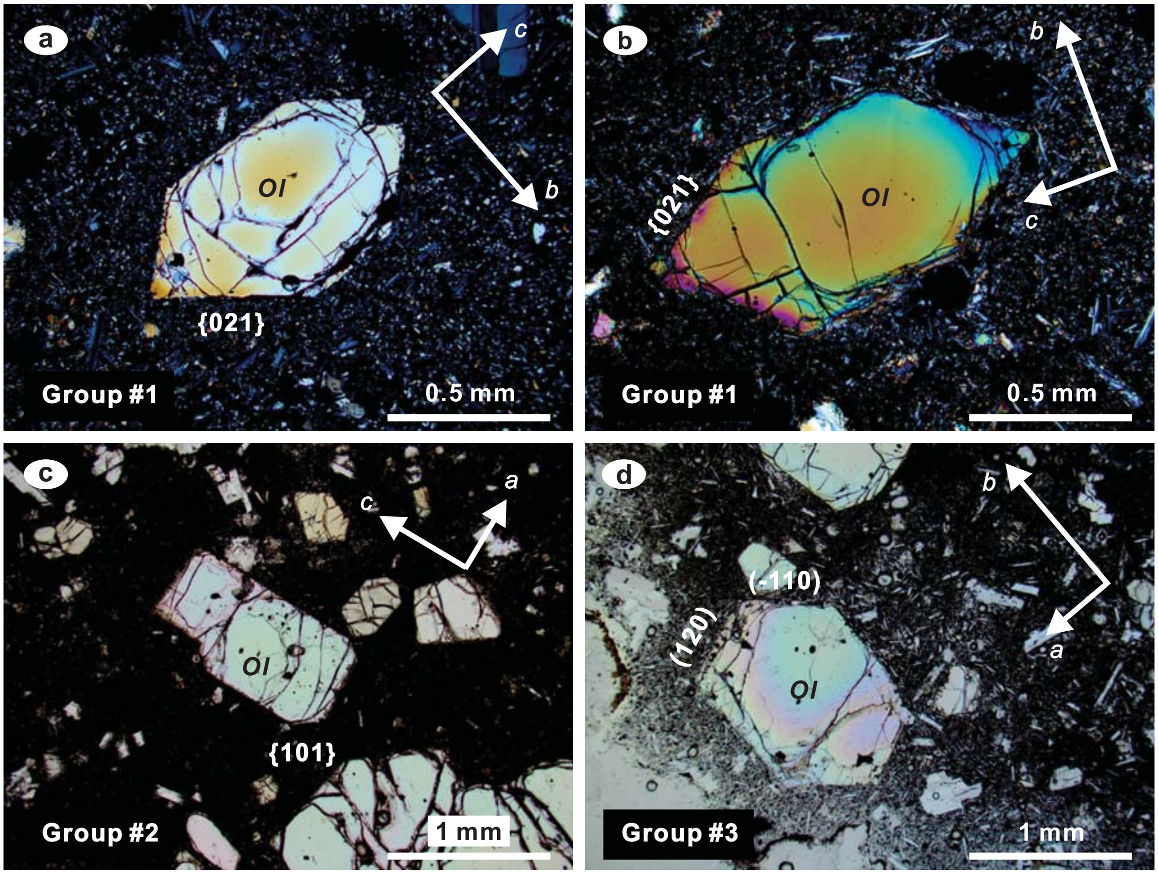
a
c
b
Ol
{021}
Group #1
0.5 mm
b
b
c
{021}
Ol
Group #1
0.5 mm
c
c
a
Ol
{101}
Group #2
1 mm
d
b
(-110)
(120)
a
Ol
Group #3
1 mm

Fig. 3

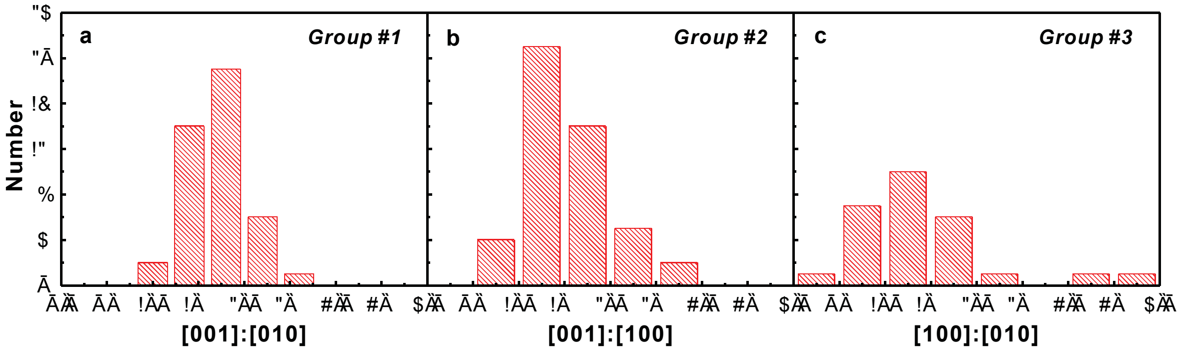

Fig. 4

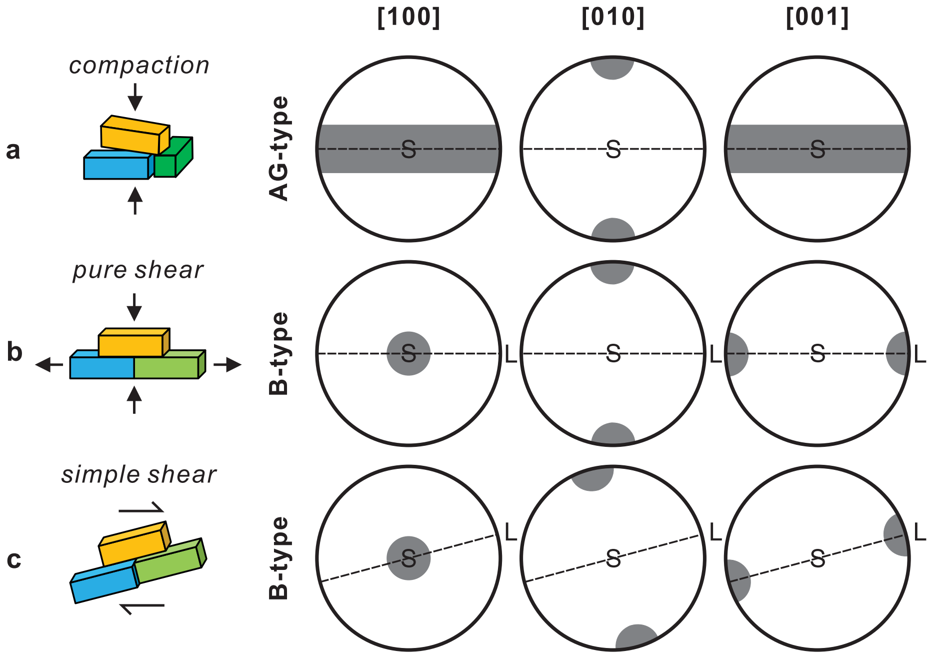
[100]
[010]
[001]
compaction
a
AG-type
S
S
S
pure shear
b
B-type
S
L
S
L
S
L
simple shear
c
B-type
S
L
S
L
S
L

Fig. 5